Actuator Fault Detection Under Active Disturbance Rejection Control for Steer-by-Wire Systems

Zoltán Téczely
Department of Control Engineering and Information Technology Budapest University of Technology and Economics
Budapest, Hungary
teczely@iit.bme.hu

Barnabás Finta
Department of Control Engineering and Information Technology Budapest University of Technology and Economics
Budapest, Hungary
finta.barnabas@edu.bme.hu

Bálint Kiss
Department of Control Engineering and Information Technology Budapest University of Technology and Economics
Budapest, Hungary
bkiss@iit.bme.hu

***Abstract*—In this paper, we present a simultaneous disturbance rejection control strategy and a fault detection, isolation, and recovery (FDIR) case study for a Steer-by-Wire (SbW) system. Since Active Disturbance Rejection Control (ADRC) lumps all disturbances into a common estimate, we propose a method that distinguishes between components to be rejected and potential safety hazards arising from actuator faults. The residual of actuator failure is distinguished by means of a correlation-based metric between the actuator effort and the estimated total disturbance. On the recovery side, the SbW system requires a master/master design architecture with two actuator sides operating in a hot-redundant condition, which allows for a near-seamless transition to a one-sided fallback operation. The applicability of the method is validated in a simulation environment, based on a real-life system with a proven background.**

***Index Terms*—Active disturbance rejection control, Steering system, Actuator fault, FDIR**

I. Introduction

Safety has been in the limelight of the automotive industry for decades, and with the increasing level of vehicle autonomy, new challenges have emerged. Steer-by-Wire (SbW) systems are in the centre of research efforts today, and with that, the traditional application of the ISO26262 automotive standard is in desperate need of a revision [1]. In SbW systems, the steering column is replaced with communication lines that provide an electrical connection between the Feedback Actuator (FBA) and the roadwheel actuator (RWA) [2]. The increased need for high controller performance, along with a range of comfort-related functions, requires the handling of external disturbances that originate from a series of sources with overlapping characteristics. Such effects are, by standard procedure, treated within the scope of robustness, ultimately reducing achievable performance.

Although disturbances affecting the steering rack are not directly fed back to the steering wheel, their effects can be wrongly perceived as faulty operation and vice versa. Fault-tolerant and fail-operational control are among the most sought-after strategies in by-wire technology, requiring an investigation to achieve ASIL-like safety qualification, which, in turn, enables mass production and consumer trust. The most obvious solution is redundancy and a well-designed fault detection, isolation and recovery (FDIR) strategy.

We propose to handle these issues under a unified framework, in which we apply Active Disturbance Rejection Control [3] for high-performance steering rack position control and disturbance attenuation objective, while being fail-operational by means of redundant actuator design and a fault detection and isolation scheme.

ADRC is frequently considered as the successor to classical control paradigms [4], [5]. It has been successfully applied in a wide range of systems, including automotive [6] and robotics [7] applications. Despite this, research on steering in academia remains scarce, with some exceptions, including [8], which can be considered as a direct precursor of the current paper. Moreover, ADRC has been analysed to counter disturbances in a lane keeping scenario in [9] and a dual-motor SbW system, along with its shortcomings, including poor tracking performance and synchronisation issues in [10]. On the other hand, fault-tolerant operation against sensor failures is presented in [11], while actuator and sensor faults are handled in [12].

The main contribution is a simultaneous residual-based fault detection strategy superimposed on the ADRC control. The application of ADRC to the SbW system allows for high-performance operation while rejecting unwanted external disturbances. On top of that, actuator defects that might be mistaken for disturbances are effectively distinguished, which enables the system to perform a state transition to a one-sided fallback operational scenario. The simplified mathematical model of the anticipated actuator fault is utilised to tell the difference between the fault and disturbance. This work is a natural successor to [13], while actuator-level control for the same system has been presented in [14].

The remainder of the paper is organised as follows. Section II gives an overview of the steering system architecture and disturbance characterisation. Section III presents the application of the ADRC control design, while Section IV introduces the fault detection strategy. In Section V, verification methodology and simulation results are given. Finally, Section VI concludes the paper.

II. System Architecture and Disturbance Characterisation

A. System Description

The SbW system consists of two subsystems - the roadwheel actuator (RWA) and the feedback actuator (FBA), described by

$$\begin{aligned}\dot{\phi}_p &= \omega_p,\\ J_p\dot{\omega}_p &= -b_p\omega_p + \tau + \frac{1}{i_m}d.\end{aligned} \tag{1}$$

and

$$\begin{aligned}\dot{\phi}_{st} &= \omega_{st},\\ J_{st}\dot{\omega}_{st} &= -b_{st}\omega_{st} + \tau_{st} + d_{drv},\end{aligned} \tag{2}$$

for the RWA and the FBA, respectively, where $\phi_.$ and $\omega_.$ are angles and angular speeds reduced to the motor, $b_.$ is a damping coefficient, $\tau_. \in \mathbb{R}$ is the control input, i_m is a transmission parameter, and $J_.$ is the inertia, with subscripts p and st denoting the RWA and the FBA, respectively. Here, d includes all load-side external disturbances and d_{drv} is the driver input torque.

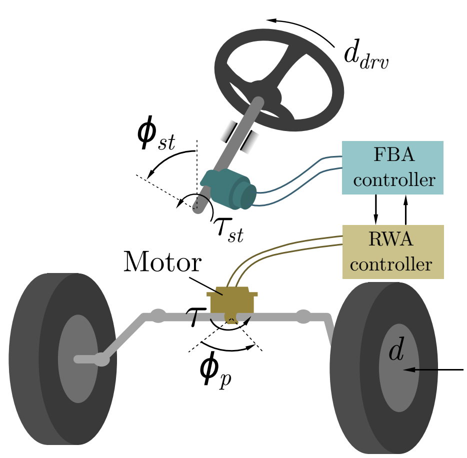

Fig. 1: Steer-by-Wire system layout.

All external disturbances under investigation enter the same channel as the input (matched condition), accommodating the ADRC philosophy.

B. Disturbance Characterisation

Typical disturbance effects entering the RWA include, but are not limited to

- High-frequency road disturbances: Forces transferred from uneven road surfaces, predominantly above 10 Hz.
- Low-frequency load torque: The base of the counteracting force from the road originating from vehicle mass, self-aligning torque, road bank, and vehicle state-dependent load transfer, typically below 5 Hz. It can be modelled as a nonlinear function of the road wheel angle, extended with simple to sophisticated tyre models (e.g. Pacejka) and suspension models.
- Shimmy: High-frequency oscillation typically in the 10–20 Hz range, caused by wheel imbalances or suspension geometry.
- Dry-friction: static Coulomb-type with negligible additional effects. The viscous element is captured in the linear model through the damping term $b_p\omega_p$.

III. Control Design

Given the disturbance characterisation and the plant dynamics of the RWA, we apply ADRC to the system (1).

A. ADRC Control Strategy

Consider the dynamic system

$$\begin{aligned}\dot{x}_1 &= x_2\\ \dot{x}_2 &= x_3\\ &\vdots\\ \dot{x}_n &= \alpha u + d\end{aligned} \tag{3}$$

where $x \in \mathbb{R}^n$ is the vector of states, α is a gain constant, $u \in \mathbb{R}$ is the control input and $d \in \mathbb{R}$ is the disturbance input. For the disturbance, we assume boundedness with $k_0 \dots k_p$ up to the p^{th} derivative, i.e.,

$$|d(t)| < k_0 \dots |d^{(p)}(t)| < k_p \qquad \forall t \in \mathbb{R}.$$

The goal of ADRC is to robustly follow a reference trajectory r with the output $y = x_1$. Let us define the tracking error as $e_1 = r - y$. Then, one can construct the tracking error dynamics as

$$e_1^{(n)} + \lambda_1 e_1^{(n-1)} + \cdots + \lambda_n e_1 = 0, \tag{4}$$

where the λ_i, $i = 1, \dots, n$, constants are design parameters. Choosing them such that all the roots of the characteristic polynomial of (4) are on the open left half plane ensures that the tracking error decays exponentially.

Since

$$e_1^{(n)} = r^{(n)} - y^{(n)} = r^{(n)} - \alpha u - d, \tag{5}$$

the control law

$$u = \frac{1}{\alpha}\left(r^{(n)} + \lambda_1 e_1^{(n-1)} + \cdots + \lambda_{n-1} e_1 - d\right) \tag{6}$$

by [3] exactly achieves (4).

Since we do not have measurements other than $y = x_1$, to implement (6) we need to provide the estimation of x_i, $i = 2, \dots, n$ and the estimation of d. To this aim, we introduce the Extended State Observer (ESO) for the system (3), as

$$\begin{aligned}\dot{\hat{x}}_1 &= \hat{x}_2 + \gamma_1(y - \hat{x}_1)\\ &\vdots\\ \dot{\hat{x}}_n &= \alpha u + z_0 + \gamma_n(y - \hat{x}_1)\\ \dot{z}_0 &= z_1 + \gamma_{n+1}(y - \hat{x}_1)\\ &\vdots\\ \dot{z}_p &= \gamma_{n+p+1}(y - \hat{x}_1).\end{aligned} \tag{7}$$

The observation errors are defined as $\hat{e}_i = x_i - \hat{x}_i$ for the states and $\hat{e}_{d,0} = d - z_0$, $\hat{e}_{d,k} = d^{(k)} - z_k$ for the k^{th} derivative of the disturbance. Substituting $\hat{x}_i, \hat{d}$ for x_i, d in (6), the error dynamics of the closed-loop system consisting of the tracking and observation errors read

$$\begin{aligned} \dot{e}_1 &= e_2 \\ \dot{e}_2 &= e_3 \\ &\vdots \\ \dot{e}_n &= -\lambda_1(e_{n-1} - \hat{e}_{n-1}) + \cdots + \hat{e}_{d,0} \\ \dot{\hat{e}}_1 &= \hat{e}_2 - \gamma_1 \hat{e}_1 \\ &\vdots \\ \dot{\hat{e}}_n &= -\gamma_n \hat{e}_1 + \hat{e}_{d,0} \\ \dot{\hat{e}}_{d,0} &= -\gamma_{n+1} \hat{e}_1 + \hat{e}_{d,1} \\ &\vdots \\ \dot{\hat{e}}_{d,p} &= -\gamma_{n+p+1} \hat{e}_1 + d^{(p)}. \end{aligned} \tag{8}$$

With $e = \begin{bmatrix} e_1 & \dot{e}_1 & \dots & e_1^{(n-1)} \end{bmatrix}^T = \begin{bmatrix} e_1 & e_2 & \dots & e_n \end{bmatrix}^T$ and $\hat{e} = \begin{bmatrix} \hat{e}_1 & \dots & \hat{e}_n & \hat{e}_{d,0} & \dots & \hat{e}_{d,p} \end{bmatrix}^T$, (8) can be written compactly as

$$\frac{d}{dt}\begin{bmatrix} e \\ \hat{e} \end{bmatrix} = \begin{bmatrix} A_r & A_{ro} \\ 0 & A_o \end{bmatrix}\begin{bmatrix} e \\ \hat{e} \end{bmatrix} + \begin{bmatrix} 0 \\ B_o \end{bmatrix} d^{(p)}, \tag{9}$$

where A_r, A_{ro}, A_o, B_o have canonical forms, containing the vectors λ, and γ.

The system matrix of (8) is an upper triangular block matrix, meaning that its eigenvalues are the union of the eigenvalues of A_r and A_o, which can be designed along the logic of the separation principle. While with input disturbances the principle does not hold, the closed-loop system can be shown to be BIBO stable. Since we know that $d^{(p)}$ is bounded according to our assumptions and if the λ_i and γ_j values are chosen such that A_r and A_o are Hurwitz, then (8) is globally asymptotically stable, the error converges to an arbitrarily small neighbourhood of the origin.

IV. Fault Detection, Isolation and Recovery

The system (3) is parameterised with an actuator-related coefficient α describing effectiveness. In this section, we propose an FDIR architecture, wherein actuator malfunctions are detected and distinguished from external disturbances to enable fault-tolerant control.

A. Disturbance Attenuation Allocation

We consider rack position control in autonomous mode, but tactile feedback to the driver follows naturally. The block diagram of the complete Steer-by-Wire system is presented in Fig. 2. The external disturbances d acting on the RWA are estimated by the ESO as $\hat{d} := z_0$, which are then used by the controller to counteract their effects. The signal $\hat{d}$ is also passed to a low-pass filter (LPF) to construct the torque provided by the FBA to the driver.

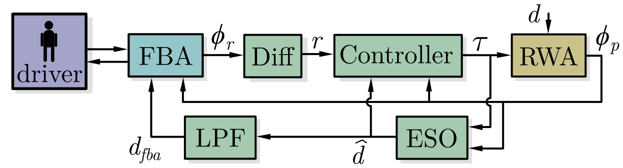

Fig. 2: System architecture block diagram.

B. Actuator Fault Modelling

We consider the nominal system dynamics (3) where $\alpha > 0$ denotes the input gain. Actuator faults directly affect the input channel as

$$\dot{x}_n = (\alpha + \Delta\alpha)\, u + d, \tag{10}$$

where $\Delta\alpha$ represents the loss of effectiveness in the power drive. Rearranging to group the disruptive effects yields

$$\dot{x}_n = \alpha u + \big(d + \Delta\alpha u\big), \tag{11}$$

where actuator faults appear inside the generalised disturbance. Since the ESO in (7) estimates the unknown input acting on the system dynamics through the observer state z_0, the disturbance estimate, under sufficiently fast dynamics, satisfies

$$\hat{d} \approx d + \Delta\alpha u. \tag{12}$$

which, under healthy operating conditions, i.e., $\Delta\alpha = 0$, reduces to $\hat{d} \approx d$.

Thus, actuator faults are embedded within the estimated disturbance signal (12) and the ESO cannot distinguish them from external disturbances. The direct proportionality of $\Delta\alpha u$ to u will be exploited for fault isolation, with the introduction of the following assumption:

Assumption 1. *Over the observation window $[t - T, t]$, the external disturbance d is weakly aligned with the control input u in the least-squares sense, i.e.,*

$$\left| \frac{\int_{t-T}^{t} d(\tau) u(\tau) d\tau}{\int_{t-T}^{t} u^2(\tau) d\tau} \right| \ll 1,$$

To justify this, let us follow the closed-loop effect paths: d enters (1), affecting the states x, whose information is used in the ESO to provide $\hat{d}$, which, in turn, is included in (6), also influenced by the control gains λ and controller order (n). r and d, by construction, are also weakly correlated, and their relationship is a function of vehicle state and road feedback. On the other hand, actuator faults enter directly through the control channel as a scaling parameter $\Delta\alpha$.

C. Structured Residual Calculation

To identify the appearance of a control-related actuator residual, we compute the coefficient that best approximates $\hat{d}$ by a scaled version of u over a finite observation window $[t - T, t]$. This is formulated as the moving least-squares problem

$$\min_{\kappa} \int_{t-T}^{t} \big(\hat{d}(\tau) - \kappa u(\tau)\big)^2 d\tau. \tag{13}$$

Equivalently, in geometric terms, we aim to find the projection of $\hat{d}(\tau)$ onto $u(t)$, i.e.,

$$\hat{\kappa}(t) := \text{proj}_u(\hat{d}) = \frac{\langle \hat{d}, u\rangle}{\langle u, u\rangle}. \tag{14}$$

Since $\langle u, u\rangle = \int u^2(\tau)d\tau$, the quadratic term represents the energy of the control input over the observation window.

The optimal coefficient $\hat{\kappa}(t)$ is obtained by standard moving least-squares optimization, i.e., for $J = \int_{t-T}^{t} \left(\hat{d}(\tau) - \kappa u(\tau)\right)^2 d\tau$, we set $\frac{dJ}{d\hat{\kappa}} = 0$, and after expansion and performing the differentiation, we get

$$\hat{\kappa}(t) = \frac{\displaystyle\int_{t-T}^{t} \hat{d}(\tau)u(\tau)\, d\tau}{\displaystyle\int_{t-T}^{t} u^2(\tau)\, d\tau}. \tag{15}$$

Substituting the disturbance decomposition (12) into (15) results in

$$\hat{\kappa}(t) = \Delta\alpha + \frac{\int_{t-T}^{t} d(\tau)u(\tau)d\tau}{\int_{t-T}^{t} u^2(\tau)d\tau}, \tag{16}$$

that is, by Assumption 1, in the absence of $\Delta\alpha$, $\hat{\kappa}(t)$ remains small. The actuator fault residual is therefore defined as

$$r_f(t) = \hat{\kappa}(t). \tag{17}$$

and a fault is detected whenever $|r_f(t)| > \gamma_f$, where γ_f is a design threshold.

Remark 1. *The second term in* (16)*, referenced in Assumption 1, represents the projection of the disturbance d onto the control signal -* $\text{proj}_u(d) = \frac{\langle d,u\rangle}{\langle u,u\rangle}$.

D. Application to the SbW system

In our model (1), ϕ_p plays the role of x_1, i.e., we try to achieve reference tracking on the motor angle. τ is our control input, $f(x)$ is a linear damping term encapsulating flexibilities and viscous friction in the RWA system. The disturbances originate from the road and, through a transmission factor i_m, act on the rotational axis of the RWA motor. These elements reflect the structural form of (3), allowing for ADRC control design. By (1), (6), and (7), we create the closed-loop and introduce disturbance effects listed in Subsection II-B. Moreover, we introduce a sudden actuator deficiency based on (10) and calculate the residual based on (15). We exclude persistent zero control action situations to avoid numerical instability. Manoeuvre-dependent correlations are also not covered, due to a lack of credible real-life scenarios.

E. Isolation and Recovery

The control software is duplicated to operate in a master-master, i.e., hot-redundant condition. The controller (6) is implemented on each side in separate control loops, and they exchange health status information (17) through a monitoring function.

Once the actuator fault is detected, the faulty side is immediately disabled, while the healthy side continues operation, being informed of the fallback procedure. At this point, no recovery to normal operation is possible, which means chattering is by design, not possible. A modified value of α is enacted in the control law to compensate for the power loss. To avoid transient effects, the healthy side takes over gradually in a prescribed dwell time T_d, which is also the primary factor for ensuring robustness against false positives. This also means that each actuator needs to be powerful enough to keep one-sided operation; hence, immediate danger is not caused by a failure, but a persistent error triggers a central ECU alarm.

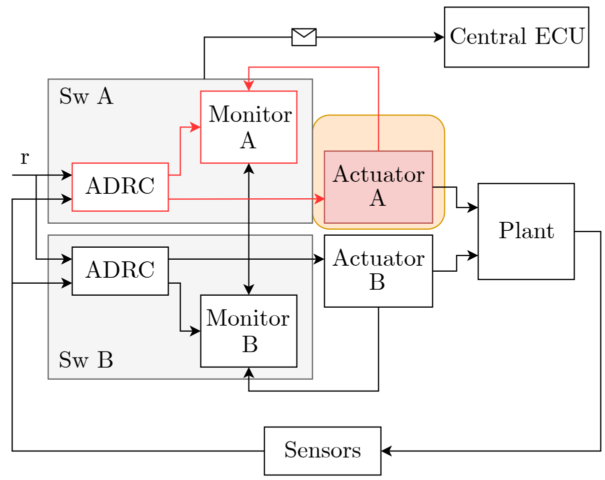

Fig. 3: System architecture under hot-redundant operation with fault injection.

For the mixed operation, two observer modes are defined:

1) a nominal observer assuming healthy redundant actuation,
2) a degraded-mode observer parameterised for single-actuator operation.

The nominal observer provides state and disturbance estimation during normal operation and is also used for fault detection. Upon fault detection, the degraded mode observer (whose internal dynamics reflect the degraded mode) is used in the controller to accurately estimate the states and disturbances in the changed dynamics. The control architecture and the switching logic are presented in Fig. 3.

V. Validation

To verify the disturbance rejection properties, the ADRC controller and corresponding ESO were compared with a standard PD-type controller. This baseline controller is henceforth denoted as *ESO off*, motivated by the fact that it can be derived from the ADRC by removing the estimated disturbance $\hat{d}$ from the control law. In addition to a range of disturbance effects, actuator faults have been injected, triggering a switchover.

The test cases were derived from vehicle use cases:

- Low-amplitude sine with increasing frequency ($0.1 - 5$ Hz)
- High-angle sine with increasing frequency ($0.1 - 5$ Hz)
- Straight run

while disturbances were defined as

- Low-frequency road feedback
- High-frequency road feedback
- Sudden burst
- Shimmy (straight run and small amplitude reference input)

Simulations were run in MATLAB/Simulink environment according to (1), (6), and (7). Residual calculation was performed according to (15) and the result was monitored against the predefined threshold (17).

The system parameters used in the simulations were

$$J_p = 5 \cdot 10^{-4} \frac{kg}{m^2}, \qquad b_p = 0.04 \frac{kg}{s}, \qquad i_m = 2400 \frac{1}{m}.$$

The ESO tuning was selected by placing the observer poles at $s_0 = -200$, which resulted in

$$\gamma_1 = 520, \qquad \gamma_2 = 78400, \qquad \gamma_3 = 9600000.$$

The controller parameters were selected as

$$\lambda_1 = 20, \qquad \lambda_2 = 100,$$

while the threshold parameter was chosen as $\gamma_f = 0.3$.

The low-frequency load was modelled as a spring-damper system with parameters $k_p = 2$, $k_v = 1$, and Coulomb-type friction with parameter $k_c = 0.5$. The shimmy phenomenon was simulated over a narrow vehicle speed range with constant amplitude and constant frequency. High-frequency road feedback was modelled as a band-limited noise with a Gaussian distribution, aligning with the usual assumptions underlying estimator design. Burst-like road disturbances were modelled as high-amplitude spikes on the disturbance channel.

A. Simulation Results

Fig. 4 presents the time-domain evaluation of the ESO through a sinusoidal test case, corresponding to high load regimes throughout the frequency range. This test case represents a common driving scenario that varies from everyday city driving through evasive manoeuvres to recreational driving.

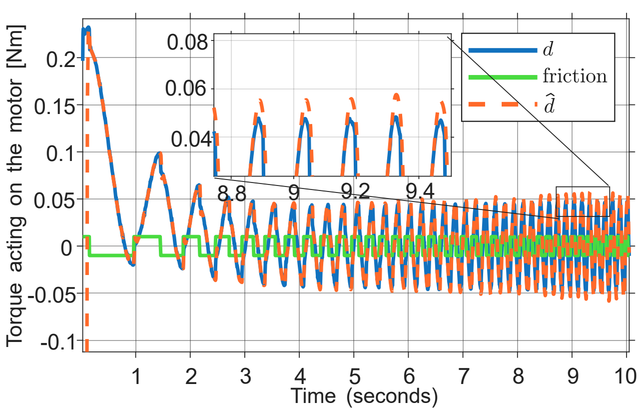

Fig. 4: Overall disturbance and its estimation. The deviation from sinusoidal character is attributed to the Coulomb friction.

After an initial transient phase, the ESO tracks the disturbance well, including the Coulomb-friction effect, as evidenced at return operating points.

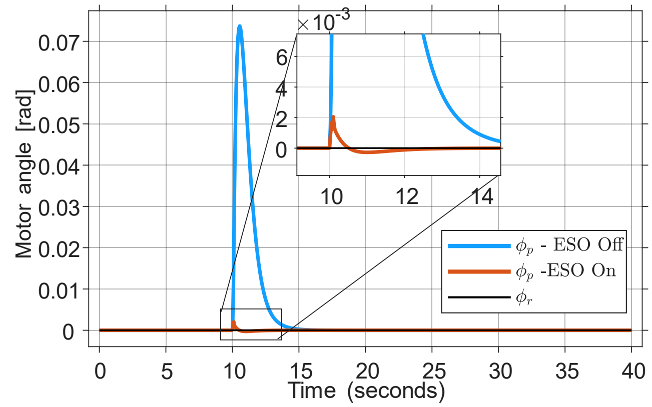

Fig. 5: Disturbance attenuation in case of ESO on/off for an impulse-like hit on the steering rack.

In Fig. 5, the reaction to an impulse-like disturbance is presented. This corresponds to potholes, bumps, and curbs on or near the road, and the behaviour describes the ESO performance and subsequent attenuation of the burst signal.

In Fig. 6, the shimmy effect is presented with and without attenuation, superimposed on a low-frequency, low-amplitude sinusoidal manoeuvre, corresponding to highway driving.

Not only is the shimmy effect visibly reduced, but a significant performance increase is also achieved. We note that perfect attenuation is not possible, since a certain disturbance level is needed to make it detectable in the first place.

In Fig. 7, the disturbance attenuation capabilities and concurrent faulty operation are presented. Up to $12s$, reference tracking for a low-frequency sinusoidal manoeuvre is nominal, actuator fault residual $\hat{\kappa}$ is low with small variance, and both actuator sides exert close to equal torques. High-frequency road feedback - in the form of bandlimited noise - is also added to the disturbance input, providing a more realistic driving scenario.

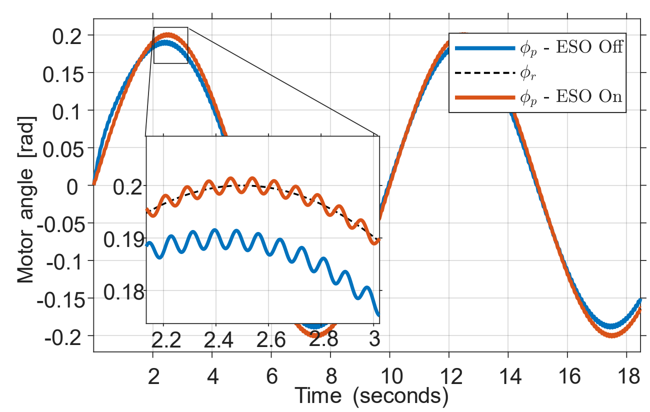

Fig. 6: Reference angle tracking in case of a small amplitude, low-frequency meandering manoeuvre.

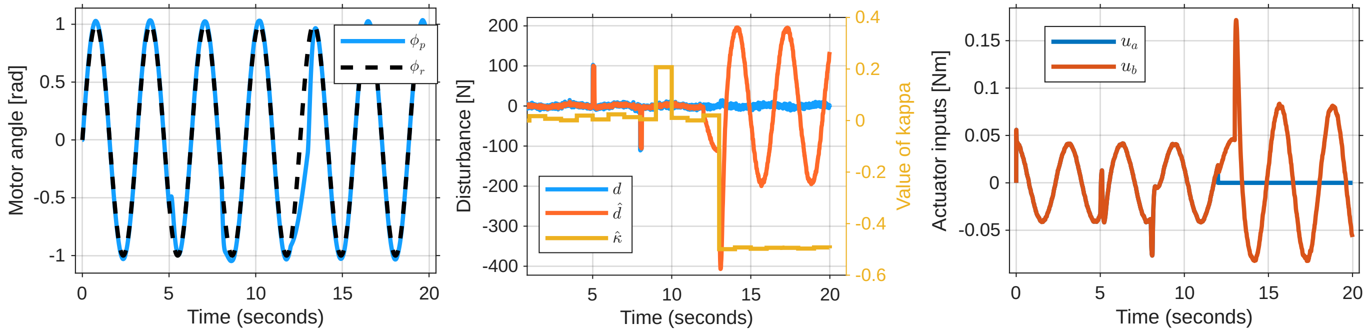

Fig. 7: Disturbance attenuation with simultaneous actuator fault injection. The fault arrives at $12s$ when actuator A completely loses power. The integration time for the fault detection system is chosen as $T = 1s$. Note the low value of $\hat{\kappa}$ even under spike disturbances and the sudden increase once the actuator fault is introduced.

Sudden bursts are injected at $5s$ and $8s$, which are estimated well by the ESO even in the presence of high-frequency noise and subsequently counteracted by control corrections, resulting in little to no performance loss. At $12s$, one side is corrupted and loses power completely, introducing a transient response in the healthy side's control input. Although this behaviour should ultimately be mitigated through appropriate transient logic, vehicle-level effects are expected to remain negligible, even in the presence of such a spike, due to the low-pass filtering nature of the chassis. This period is also characterised by reduced trajectory tracking performance, although overall tracking is maintained. During this time, $\hat{\kappa}$ changes rapidly according to (16), providing a clear distinction between sudden burst-like disturbances from the road and actuator defects. After this transient, trajectory tracking is restored by the healthy side, taking over the full control task with nominal performance. Recovery is thus, performed automatically with fast dynamics, depending on controller tuning. Independently from control action, the driver is notified by hazard lights to prevent prolonged one-sided operation.

VI. Conclusion

The results presented in this paper are indicative of the feasibility of the application of ADRC to steering systems while differentiating from faulty behaviour. As an obvious advantage, we mention improved disturbance rejection quality, allowing for increased applicability in future technologies like autonomous driving, modularisation within the automotive ECU layout, smart technologies and more. Moreover, ADRC provides an integrated solution to a wider range of objectives, as opposed to the traditional, distinct handling of trajectory tracking control and disturbance attenuation. Concurrent appearance of external disturbances and actuator faults was also considered, and a residual-based fault detection strategy was proposed, together with an FDIR scheme, which allows for fail-operational control. As a potential improvement, the ESO estimates can be further differentiated based on vehicle state and frequency content. The natural next step in validation is scheduled to be hardware-in-the-loop testing in a real-time environment and subsequently vehicle-level testing.

References

[1] P. Kilian, A. Köhler, P. Van Bergen, C. Gebauer, B. Pfeufer, O. Koller, and B. Bertsche, "Principle Guidelines for Safe Power Supply Systems Development," *IEEE Access*, vol. 9, pp. 107 751–107 766, 2021.

[2] S. A. Mortazavizadeh, A. Ghaderi, M. Ebrahimi, and M. Hajian, "Recent Developments in the Vehicle Steer-by-Wire System," *IEEE Transactions on Transportation Electrification*, vol. 6, no. 3, pp. 1226–1235, 2020.

[3] H. Sira-Ramirez, A. Luviano-Juárez, M. Ramirez-Neria, and E. Zurita-Bustamante, *Active Disturbance Rejection Control of Dynamic Systems: A flatness based approach*, 10 2018.

[4] J. Han, "From PID to Active Disturbance Rejection Control," *IEEE Transactions on Industrial Electronics*, vol. 56, no. 3, pp. 900–906, 2009.

[5] Z. Gao, "Active disturbance rejection control: a paradigm shift in feedback control system design," in *2006 American Control Conference*, 2006, pp. 7 pp.–.

[6] Y. Lu, H. Wang, and Y. Tian, "Active Disturbance Rejection Control for Active Suspension System of Nonlinear Full Car," in *2018 IEEE 7th Data Driven Control and Learning Systems Conference (DDCLS)*, 2018, pp. 724–729.

[7] M. Ramírez-Neria, H. Sira-Ramírez, R. Garrido-Moctezuma, A. Luviano-Juárez, and Z. Gao, "Active Disturbance Rejection Control for Reference Trajectory Tracking Tasks in the Pendubot System," *IEEE Access*, vol. 9, pp. 102 663–102 670, 2021.

[8] A. Rodriguez-Angeles and J. Garcia-Antonio, "Active disturbance rejection control in steering by wire haptic systems," *ISA Transactions*, vol. 53, no. 4, pp. 939–946, 2014.

[9] Z. Chu, Y. Sun, C. Wu, and N. Sepehri, "Active disturbance rejection control applied to automated steering for lane keeping in autonomous vehicles," *Control Engineering Practice*, vol. 74, pp. 13–21, 05 2018.

[10] S. Zou, W. Zhao, C. Wang, W. Liang, and F. Chen, "Tracking and Synchronization Control Strategy of Vehicle Dual-Motor Steer-by-Wire System via Active Disturbance Rejection Control," *IEEE/ASME Transactions on Mechatronics*, vol. 28, no. 1, pp. 92–103, 2023.

[11] S. A. Mortazavizadeh, M. Ebrahimi, A. Ghaderi, and M. Hajian, "Fault-tolerant control of steer-by-wire systems under voltage and current sensors faults," *Electrical Engineering*, vol. 103, pp. 1–9, 02 2021.

[12] M. Boudaoud, C. Sentouh, C. Cappelle, M. El Badaoui El Najjar, and J.-C. Popieul, "A New Observer-Based Fault Tolerant Shared Control for SbW Systems with Actuator Fault for Driver Assistance," in *2025 21st International Conference on Informatics in Control, Automation and Robotics (ICINCO)*, 01 2024, pp. 189–197.

[13] Z. Téczely, C. Fazekas, and B. Kiss, "On Synchronous Motor-Driven Mechanical Systems: Analysis and Linear Parameter-Varying Control," *IEEE Transactions on Control Systems Technology*, vol. 34, no. 3, pp. 1311–1322, 2026.

[14] Z. Téczely and D. Somogyi, "Indirect Torque Control of Synchronous Machines via Feedback Linearization," in *2025 11th International Conference on Control, Decision and Information Technologies (CoDIT)*, vol. 1, 2025, pp. 700–705.